

Prompt photon in association with a heavy-quark jet in Pb–Pb collisions at the LHC

Tzvetalina Stavreva,^a François Arleo,^b Ingo Schienbein^a

^a*Laboratoire de Physique Subatomique et de Cosmologie, UJF, CNRS/IN2P3, INPG, 53 avenue des Martyrs, 38026 Grenoble, France*

^b*Laboratoire d'Annecy-le-Vieux de Physique Théorique (LAPTh) UMR5108, Université de Savoie, CNRS, BP 110, 74941 Annecy-le-Vieux cedex, France*

E-mail: stavreva@lpsc.in2p3.fr, arleo@lapp.in2p3.fr, schien@lpsc.in2p3.fr

ABSTRACT: We present a phenomenological study of the associated production of a prompt photon and a heavy quark jet (charm or bottom) in Pb–Pb collisions at the LHC. This channel allows for estimating the amount of energy loss experienced by the charm and bottom quarks propagating in the dense QCD medium produced in those collisions. Calculations are carried out at next-to-leading order (NLO) accuracy using the BDMPS-Z heavy-quark quenching weights. The quenching of the single heavy-quark jet spectrum reflects fairly the hierarchy in the heavy quark energy loss assumed in the perturbative calculation. On the contrary, the single photon spectrum in heavy-ion collisions is only modified at low momenta, for which less heavy-quark jets pass the kinematic cuts. On top of single particle spectra, the two-particle final state provides a range of observables (photon-jet pair momentum, jet asymmetry, among others) which are studied in detail. The comparison of the photon-jet pair momentum, from p–p to Pb–Pb collisions, is sensitive to the amount of energy lost by the heavy-quarks and could therefore be used in order to better understand parton energy loss processes in the heavy quark sector.

KEYWORDS: heavy ion collisions, parton energy loss, direct photon production, heavy quark jet

Contents

1	Introduction	1
2	Theoretical framework	3
2.1	$\gamma + Q$ production in p-p collisions	3
2.2	$\gamma + Q$ production in heavy-ion collisions	4
2.3	Quenching weights	5
2.4	Observables	6
3	Results	8
3.1	Ingredients	8
3.2	Total cross sections and event rates	9
3.3	Single-inclusive transverse momentum spectra	10
3.3.1	Differential cross sections	10
3.3.2	Quenching factors R_{AA}	11
3.4	Two-particle observables	14
4	Conclusions	17

1 Introduction

Spectacular experimental results on large p_T particle production have been reported in Pb–Pb collisions at the LHC by the ALICE, ATLAS, and CMS experiments. The quenching of light hadrons (inclusive charged hadrons, pions, etc.) has been observed over a very large range of transverse momenta [1–3], soon followed by that of charmed mesons such as D or D^* [4, 5]. Apart from large- p_T hadron production, the reconstruction of jets in heavy-ion collisions also allowed for the observation of significant jet asymmetries of jet–jet [6, 7], photon–jet [8] and Z–jet [9] correlations, as well as measurements of hadron momentum spectra (the so-called fragmentation functions) inside jets [10, 11].

Clearly, these results are qualitatively consistent with parton energy loss processes as hard quarks and gluons propagate through the dense QCD medium produced in those collisions. On the more quantitative side many questions still remain unanswered, among which the issue of (radiative) energy loss in the heavy quark sector. Because the heavy quark mass acts as a collinear cut-off in the medium-induced gluon radiation, the following hierarchy $\epsilon_q > \epsilon_c > \epsilon_b$ of the typical energy loss of light, charm and bottom quarks has been proposed by Dokshitzer and Kharzeev [12] and later checked by Armesto, Salgado and Wiedemann in the BDMPS-Z energy loss framework [13]. Experimentally, however, the slight differences in the quenching of D mesons with respect to that of pions might nevertheless be understood as coming from the different color charge of the propagating

parton, essentially heavy quarks ($C_F = 4/3$) and gluons ($C_A = 3$) for D mesons and pions, respectively. As of today, there is no clear and indisputable sign on possible differences between the energy loss of light and heavy quarks. On the theoretical side, moreover, the above “standard” hierarchy has also been recently questioned by Aurenche and Zakharov in Ref. [14] due to formation time effects. It is therefore crucial to identify observables at the LHC which could help clarify this issue. In this paper, we argue that measuring prompt photon production in association with a heavy quark tagged jet (denoted as $\gamma + Q$ in the following) in heavy-ion collisions might shed light on the mass dependence of the radiative parton energy loss mechanism.

The production of $\gamma + Q$, first measured in $p\text{--}\bar{p}$ collisions at the Tevatron by the D0 and CDF experiments [15–18], is a rich and versatile process in various hadronic collisions:

- In $p\text{--}p$ and $p\text{--}\bar{p}$ collisions, first of all, $\gamma + Q$ production offers sensitive checks of perturbative QCD (pQCD) and might serve as a probe of intrinsic heavy quark distributions inside the proton [19];
- In $p\text{--}A$ collisions (e.g. at RHIC and soon at the LHC), this process can be used to constrain the gluon parton distribution function in nuclei (nPDF) [20], which is pretty much unconstrained at small values of x . One should underline that knowing precisely the nuclear PDFs is a prerequisite in order to obtain reliable predictions in heavy-ion collisions;
- In $A\text{--}A$ collisions, finally, the study of $\gamma + Q$ provides an ideal tool for investigating the energy lost by heavy quarks in the hot QCD medium produced in those collisions. Being an electromagnetic probe, the photon produced directly in the hard process is expected to traverse the medium unaffected. Its momentum can therefore serve as a proxy for the initial momentum of the heavy quark propagating through the dense medium and eventually fragmenting into the heavy quark jet. The imbalance between the prompt photon and the heavy quark jet momentum going from $p\text{--}p$ to $A\text{--}A$ collisions might thus reflect the amount of energy loss experienced by the heavy quark. Furthermore, the comparison between $\gamma + c$ and $\gamma + b$ production would provide access to the mass hierarchy of parton energy loss.

It is the purpose of this paper to perform an exploratory study of heavy quark energy loss from a next-to-leading order (NLO) QCD analysis of $\gamma + Q$ production in heavy-ion collisions.¹ In addition to the photon and the heavy quark p_T spectra, we study the distributions in different kinematic variables (q_T , A_J , z) which prove useful in order to characterize the amount of heavy quark energy loss in the medium. Note that in these latter cases, it is mandatory to perform the theoretical calculation of the $\gamma + Q$ production process at NLO in order to obtain reliable results since these variables exhibit a singular behavior at LO accuracy. However even for the more inclusive observables such as the

¹A related but different analysis of prompt photon and heavy quark *hadrons* has been performed previously at LO accuracy in the fixed-flavor number scheme [21]. Earlier studies investigating photon correlations with inclusive hadrons have been performed at NLO, see e.g. [22, 23]. More recently γ correlations with inclusive jets were also investigated [24].

p_T -distributions of either the photon or the heavy quark, which are not singular at LO, the NLO calculation is important for obtaining the right magnitude of the cross section. As we shall see in Section 2.2, however, the treatment of parton energy loss processes in heavy-ion collisions is performed at leading order only.

This paper is organized as follows. In Section 2 we describe our theoretical framework for the $\gamma + Q$ production including the effects of the medium formed during the A–A collisions. Our numerical results are presented in Section 3. Finally, in Section 4 we present our conclusions and give an outlook on possible future improvements of the analysis.

2 Theoretical framework

2.1 $\gamma + Q$ production in p–p collisions

Using the standard pQCD collinear factorization framework the cross section for the production of a photon and a heavy quark in p–p collisions is given by

$$d\sigma = \sum_{i,j,k} f_i \otimes f_j \otimes d\hat{\sigma}(ij \rightarrow kQ) \otimes D_k^\gamma, \quad (2.1)$$

where the sum over all possible partonic subprocesses is performed and f_i stands for the parton distribution function in the proton. Furthermore, D_k^γ describes the fragmentation of the final state parton k into the observed photon and the direct contribution ($k = \gamma$) is included via $D_\gamma^\gamma(z) = \delta(1 - z)$.

The contributing partonic subprocesses depend on the heavy flavor scheme. The present calculation is performed in the variable flavor number scheme (VFNS), which includes heavy quark PDFs for factorization scales greater than the threshold given by the heavy quark mass, $\mu_F \geq m_Q$. Furthermore, heavy quark mass terms m_Q^2/μ^2 have been neglected in the perturbative calculation of the partonic cross sections where the factorization/renormalization scale μ is identified with a typical hard scale of the process, that is the transverse momentum of the photon or the jet.² The range of validity of the calculation is thus restricted to momenta $\mu = \mathcal{O}(p_T)$ larger than a few times the heavy quark mass. Note that in heavy-ion collisions the factorization ansatz in Eq. (2.1) is a working assumption.

$gg \rightarrow \gamma Q \bar{Q}$	$gQ \rightarrow \gamma g Q$
$Qq \rightarrow \gamma q Q$	$Q\bar{q} \rightarrow \gamma \bar{q} Q$
$Q\bar{Q} \rightarrow \gamma Q \bar{Q}$	$QQ \rightarrow \gamma QQ$
$q\bar{q} \rightarrow \gamma Q \bar{Q}$	

Table 1. List of all direct $2 \rightarrow 3$ NLO hard-scattering subprocesses.

At leading-order accuracy, $\mathcal{O}(\alpha\alpha_s)$, the production of a *direct* photon with a heavy quark jet only arises from the $gQ \rightarrow \gamma Q$ Compton scattering subprocess at the hard-

²Note that in the case of a gluon splitting into a collinear $Q\bar{Q}$ pair, the divergency is avoided by imposing a cut on the invariant mass such that $m_{Q\bar{Q}} > 2m_Q$ [19].

scattering level. At next-to-leading order, however, the number of contributing subprocesses increases to seven (see Table 1). On top of these direct photon subprocesses, the contributions coming from the fragmentation of a parton into a photon are also included consistently at NLO accuracy. It should however be mentioned that isolation requirements – used experimentally in order to minimize background coming from hadron decays – greatly decrease these fragmentation contributions. For further details on the theoretical calculations, the reader may refer to [19, 25].

2.2 $\gamma + Q$ production in heavy-ion collisions

We discuss in this section the calculation of $\gamma + Q$ production in heavy-ion collisions, in which the final-state partons propagating through the dense QCD medium are expected to lose energy through medium-induced gluon radiation, or *radiative* energy loss processes.³

Let us first denote by p_Q^{vac} and p_γ^{vac} the 4-momenta of the heavy quark and the photon, respectively, in p–p collisions. We express these momenta in terms of their transverse momentum p_T^{vac} and rapidity y^{vac} :

$$p_Q^{\text{vac}} = p_{TQ}^{\text{vac}}(\cosh y_Q^{\text{vac}}, \vec{e}_{TQ}, \sinh y_Q^{\text{vac}}), \quad (2.2)$$

$$p_\gamma^{\text{vac}} = p_{T\gamma}^{\text{vac}}(\cosh y_\gamma^{\text{vac}}, \vec{e}_{T\gamma}, \sinh y_\gamma^{\text{vac}}). \quad (2.3)$$

Because of energy loss processes, in heavy-ion collisions the energy of the heavy quark is shifted with respect to that in p–p collisions, $E_Q = E_Q^{\text{vac}} - \epsilon$, where ϵ is the amount of energy lost by the heavy quark while traversing the medium.⁴ In the present exploratory study, we assume that the photon is not affected by the medium, $E_\gamma = E_\gamma^{\text{vac}}$, and moreover that the heavy quark does not change its direction while propagating through the medium, $y_Q = y_Q^{\text{vac}}$. Therefore, the heavy quark momentum in the medium is given by

$$p_Q = p_{TQ}(\cosh y_Q, \vec{e}_{TQ}, \sinh y_Q) = [p_{TQ}^{\text{vac}} - \epsilon / \cosh y_Q^{\text{vac}}](\cosh y_Q^{\text{vac}}, \vec{e}_{TQ}, \sinh y_Q^{\text{vac}}), \quad (2.4)$$

i.e.,

$$p_{TQ} = p_{TQ}^{\text{vac}} - \epsilon_T, \quad \epsilon_T = \epsilon / \cosh y_Q^{\text{vac}}. \quad (2.5)$$

As discussed in the previous section, beyond the leading order a second parton (labeled “2”) is produced in real $2 \rightarrow 3$ subprocesses (see Table 1). The emission of this extra parton occurs within the short-distance time scale $\mathcal{O}(Q^{-1}) \ll 1$ fm (where $Q \gg \Lambda_{\text{QCD}}$ is the scale of the hard process), therefore well *before* the medium is produced. As a consequence, parton 2 also experiences medium-induced energy loss; its energy is thus shifted, $E_2 = E_2^{\text{vac}} - \epsilon'$, leading to the following expression for its momentum in medium similar to (2.4),

$$\begin{aligned} p_2 &= [p_{T2}^{\text{vac}} - \epsilon' / \cosh y_2^{\text{vac}}](\cosh y_2^{\text{vac}}, \vec{e}_{T2}, \sinh y_2^{\text{vac}}), \\ p_{T2} &= p_{T2}^{\text{vac}} - \epsilon'_T, \quad \epsilon'_T = \epsilon' / \cosh y_2^{\text{vac}}, \quad y_2 = y_2^{\text{vac}}, \end{aligned} \quad (2.6)$$

³We do not consider collisional energy loss processes in this study, as they are expected to be less important (in comparison to radiative losses) at large momenta.

⁴Strictly speaking, ϵ should be understood as the energy radiated *outside* the jet cone. We therefore implicitly assume in the present study that most of the medium-induced gluon radiation occurs at large angles.

after losing the energy ϵ' in the medium.

Although the dynamics of $\gamma + Q$ production is performed at NLO in order to get meaningful results for the 2-particle distributions, we stress that energy loss processes are treated at leading order accuracy. In particular the momenta of the two final-state partons produced in $2 \rightarrow 3$ processes are shifted *independently*. In doing so we neglect the possible interference effects in the medium-induced gluon radiation off two partons. This question has been addressed in a recent series of papers, see for example [26] as well as [27] for the treatment involving massive partons. Completing the NLO treatment of this process by including the energy loss coherence effects is of great interest, and will be the aim of a future study. There, also the issue of subsequent (soft and collinear) radiation can be addressed, these occurring on longer time scales and possibly after the radiating parton has escaped the medium (see [28]); such radiation, which might be more sensitive to the above coherence effects, is not taken into account in the present fixed-order calculation scheme but could rather be studied through Monte Carlo parton showers. A recent discussion on coherence effects on the jet evolution in a medium can be found in [29].

Note that the energy loss of the extra parton affects the production of $\gamma + Q$ events as long as it is recombined with the heavy quark Q to form the heavy-flavor jet through a jet reconstruction algorithm⁵, and not otherwise.

In order to compute the medium-modified $\gamma + Q$ production cross section in heavy-ion collisions, we use the following Monte Carlo procedure:

1. We obtain an event for the production of a $\gamma + Q$ in vacuum at a given heavy quark four momentum p_Q^{vac} and photon four momentum, p_γ^{vac} .
2. For each partonic event (i.e. with one or two partons in the final state), the energy loss ϵ (respectively, ϵ') of the heavy quark (respectively, the extra parton) is sampled according to a probability distribution or *quenching weight*, $\mathcal{P}_i(\epsilon)$, using an acceptance-rejection algorithm.
3. According to Eqs. (2.4) and (2.6), medium-modified four-momenta p_Q , p_γ and p_2 are constructed. The additional constraints, $\epsilon < E_Q^{\text{vac}}$ and $\epsilon' < E_2^{\text{vac}}$, are moreover imposed.
4. Using the modified four-vectors we evaluate observables $(p_{TQ}, p_{T\gamma})$, as well as the correlation variables discussed in Sec. 2.4 in which we bin the events, providing the differential cross section for these observables.

2.3 Quenching weights

The quenching weights used in the present calculation are obtained using the Poisson approximation proposed in [30],

$$\mathcal{P}_j(\epsilon) = \sum_{n=0}^{\infty} \frac{1}{n!} \left[\prod_{i=1}^n \int_0^\epsilon d\omega_i \frac{dI(\omega_i)}{d\omega} \Big|_j \right] \times \delta \left(\epsilon - \sum_{i=1}^n \omega_i \right) \exp \left\{ - \int_0^\infty d\omega \frac{dI}{d\omega} \right\}, \quad (2.7)$$

⁵ For the jet reconstruction we combine the heavy quark and parton 2 in a jet if they are within a cone of radius R specified in Table 2.

where j is the flavor of the propagating parton ($j = q, g, Q$) and $dI/d\omega$ the medium-induced gluon spectrum, which in the present work is determined from the perturbative BDMPS-Z framework [31].

The quenching weights $\mathcal{P}_j(\epsilon)$ are a scaling function of ϵ/ω_c , where $\omega_c \equiv 1/2 \hat{q} L^2$ is the typical scale for the energy loss process; the transport coefficient \hat{q} measures the scattering power of the medium (momentum broadening per unit length) and L is the medium length. The medium-induced gluon spectrum (and therefore the quenching weights) depends on the dimensionless parameter R , $R \equiv \omega_c L$, which arises from the kinematic constraint restricting the transverse momenta of the radiated gluons. The limit $R \rightarrow \infty$ of the spectrum corresponds to the “thick medium” limit of the BDMPS formulation [32] in which the opacity, or the number of rescatterings $n = L/\lambda \rightarrow \infty$.⁶

In our numerical analysis we use the quenching weights provided in [33] for massless quarks and gluons and in [34] for heavy quarks. In the latter case, the weights also depend on the heavy quark mass through the dimensionless quantity m/E , where E is the heavy quark energy in the medium rest frame. In this exploratory study, we will stick to the BDMPS framework, i.e. using the quenching weights computed in the multiple scattering scenario (as opposed to the $n = 1$ opacity case) and taking the “thick” limit, $R \rightarrow \infty$.⁷

Due to the heavy quark mass, the medium-induced radiation is suppressed at large gluon energies, see [13]. As a consequence, the typical energy loss in this calculation is substantially reduced when m/E is large. This calculation confirms in particular the hierarchy, $\epsilon_q > \epsilon_c > \epsilon_b$, conjectured in [12] for heavy quark energy losses in QCD media.⁸ As mentioned in the introduction, this hierarchy has recently been questioned by Aurenche and Zakharov in [14] on the basis of formation time arguments. It is not the goal of the present paper to answer this question, nor is it to perform a comprehensive phenomenological study which would encompass various assumptions regarding heavy quark energy loss and a full treatment of the geometry and the dynamics of the produced medium. Rather we explore how the properties of the medium-induced gluon radiation off massive quarks translates into a variety of $\gamma + Q$ observables through an NLO calculation — within one well defined scheme for heavy quark energy loss.

In the next section, we present the different distributions which we consider in this study that we believe would best reflect the dynamics of massive quark energy loss processes in heavy-ion collisions.

2.4 Observables

The most inclusive observable which should be sensitive to the energy loss is the total cross section in dependence of the cut on the p_{TQ} (or $p_{T\gamma}$). In addition it is useful to

⁶Note that in this limit, the probability for no energy loss vanishes.

⁷For practical purposes, in order to allow for reasonable CPU time, we use $R = 10^5$. This seems to be a good approximation since the probability for no energy loss, p_0 , is already below the few percent level for the m/E values used in the calculation.

⁸At small values of the heavy quark mass, $m/E \sim 10^{-2}$ and intermediate values $R \sim 10^3$ – 10^4 , the energy loss of massive quarks is actually *larger* than in the massive case, questioning the hierarchy $\epsilon_q > \epsilon_c > \epsilon_b$. It is however not clear in [13] whether this observation has a well defined physical origin or is an artifact of the calculation.

study the inclusive transverse momentum distributions of the heavy quark and the photon, respectively.

On top of the photon and the heavy quark jet single p_T spectra, the two-particle final state further offers a wide range of observables which might give a better access to the energy loss of the propagating heavy quark. One such variable is the transverse momentum difference between the photon and the heavy quark jet, q_T , defined as follows:

$$q_T = p_{T\gamma} - p_{TQ}. \quad (2.8)$$

At leading order and assuming that the photon is produced directly in the hard process (i.e. not by fragmentation), the photon and the jet momenta balance in the transverse plane. Therefore this variable reduces at LO to $q_T^{\text{vac}} = p_{T\gamma}^{\text{vac}} - p_{TQ}^{\text{vac}} = 0$ in the vacuum (p-p collisions) and $q_T^{\text{med}} = p_{T\gamma} - p_{TQ} = p_{T\gamma}^{\text{vac}} - (p_{TQ}^{\text{vac}} - \epsilon_T) = \epsilon_T$ in the medium (A-A collisions). Therefore, a non-zero cross section at a given $q_T^{\text{med}} \neq 0$ can be interpreted (at LO, direct) to be proportional to the number of events where the heavy quark jet has suffered an energy loss $\epsilon_T = q_T^{\text{med}}$ in the medium. It is unfortunately not as simple because the “vacuum” q_T distribution in p-p collisions is non-zero at $q_T > 0$ as soon as fragmentation photons or NLO contributions are taken into account (the former being however suppressed from the use of isolation criteria).

Assuming the photon and the jet to be in different hemispheres (see also the cuts in Table 2) the momentum difference in A-A collisions becomes $q_T^{\text{med}} = p_{T\gamma}^{\text{vac}} - (p_{TQ}^{\text{vac}} - \epsilon_T) = q_T^{\text{vac}} + \epsilon_T$. In other words the q_T spectrum in A-A collisions is shifted by $+\epsilon_T$ as compared to p-p collisions, where ϵ_T should be understood as a typical amount of (transverse) energy loss. The shift should therefore be more pronounced for light jets than for charm and bottom quark jets, because of the hierarchy used in the calculation.

Similar to the photon-jet pair momentum we shall investigate as well the imbalance A_J ,

$$A_J = \frac{p_{T\gamma} - p_{TQ}}{p_{T\gamma} + p_{TQ}}, \quad (2.9)$$

which has been measured for dijet [6, 7, 35] and photon-jet correlations [8] by ATLAS and CMS. Finally the distribution in the momentum imbalance,

$$z_{\gamma Q} = -\frac{\vec{p}_{T\gamma} \cdot \vec{p}_{TQ}}{p_{T\gamma}^2} \quad (2.10)$$

is also considered. In the leading order kinematics (and assuming the photon is produced directly in the hard process), these two variables would reduce respectively to $A_J^{\text{med}} = \epsilon_T / (2p_{T\gamma}^{\text{vac}} - \epsilon_T)$ and $z_{\gamma Q}^{\text{med}} = 1 - \epsilon_T / p_{T\gamma}^{\text{vac}}$ in heavy-ion collisions. As compared to the q_T variable, these are sensitive to the ratio of the energy lost over the parton energy (or, fractional energy loss), $\epsilon_T / p_{T\gamma}^{\text{vac}}$, instead of the absolute magnitude of the energy loss, ϵ_T .

Generically, for all the above observables quenching factors R_{AA} are defined as

$$R_{AA} = \frac{1}{N_{\text{coll}}} \frac{d\sigma(\text{A} + \text{A} \rightarrow \gamma + Q)}{d\sigma(\text{p} + \text{p} \rightarrow \gamma + Q)}, \quad (2.11)$$

where N_{coll} stands for the number of binary nucleon–nucleon collisions ($N_{\text{coll}} = A^2$ in minimum bias A–A collisions). In particular, we consider the suppression factors for the inclusive $p_{T\gamma}$ spectrum, $R_{AA}^\gamma(p_{T\gamma})$, and for the inclusive p_{TQ} spectrum, $R_{AA}^Q(p_{TQ})$.

Some comments are in order: (i) With this definition the ratios R_{AA}^γ and R_{AA}^Q would in general be different from unity even in the absence of cold and hot nuclear matter effects due to differences between parton distributions inside protons and neutrons as is the case for inclusive photon production (see e.g. [36]). However, in our case the dominant initial state is $g + Q$ and these parton distributions should be (to a very precise level) the same inside protons and neutrons. (ii) To construct this ratio experimentally, the p–p cross section which is measured at a different center-of-mass energy has to be extrapolated to the center-of-mass energy of the A–A run. For this reason it is extremely valuable that the photon transverse momentum spectrum which is insensitive to hot medium effects (up to a sensitivity on the cut on the heavy quark jet energy) can be used to calibrate the effects of the energy extrapolation and of cold nuclear matter. (iii) An advantage of considering the double ratios $R_{AA}^{Q/\gamma} = R_{AA}^Q/R_{AA}^\gamma$ is that uncertainties due to the choice of scales and nuclear PDFs should largely cancel. While the scale uncertainties already cancel to a good degree in the simple ratios there remains a residual uncertainty due to the lack of knowledge of the nuclear gluon distribution, see e.g., [20]. Hence, it will be crucial to use data from the upcoming p–Pb run at the LHC at the beginning of 2013 to better constrain the nuclear gluon distribution.⁹ Therefore, for the time being we refrain from using nuclear PDFs [37–40] in this study where we focus on the effects of the heavy quark energy loss solely.

3 Results

3.1 Ingredients

The present calculations have been carried out using the CTEQ6.6M PDFs inside a proton [41] (along with the corresponding strong coupling constant $\alpha_s^{\overline{\text{MS}},5}(M_Z) = 0.118$ at next-to-leading order) and the photon fragmentation functions of Bourhis, Fontannaz and Guillet [42]. The renormalization, factorization and fragmentation scales have been set to $\mu_R = \mu_F = \mu_f = p_{T\gamma}$ and we have used $m_c = 1.3$ GeV and $m_b = 4.2$ GeV for the charm and bottom quark masses. All cross sections (for both p–p and Pb–Pb collisions) have been calculated at a center-of-mass energy $\sqrt{s_{\text{NN}}} = 5.5$ TeV.

For our exploratory numerical studies, we apply the kinematic cuts provided in Table 2. Most notably, the cuts on the minimal $p_{T\gamma}$ and p_{TQ} are asymmetric in order to avoid configurations with $p_{T\gamma} \simeq p_{TQ}$ where the NLO cross section is known to become infrared sensitive [20]. For simplicity, we consider events at mid-rapidity in small bins around $y_\gamma = 0$ and $y_Q = 0$. Moreover we impose a cut on the azimuthal angle between the photon and heavy quark jet, $\Delta\phi_{\gamma Q} > 3\pi/4$ in order to ensure that the photon and the heavy quark are produced in different hemispheres. Once data are available with sufficient statistics these results could be updated with the appropriate experimental cuts.

⁹Alternatively, constraints on the nPDFs could possibly be obtained through *inclusive* photon and weak boson production in A–A collisions.

	p_T	Rapidity	Photon isolation	Jet radius
Photon	$p_{T,\gamma}^{min} = 20 \text{ GeV}$	$ y_\gamma < 0.2$	$R = 0.4, \epsilon < 0.1E_\gamma$	—
Heavy quark jet	$p_{T,Q}^{min} = 12 \text{ GeV}$	$ y_Q < 0.2$	—	$R = 0.4$

Table 2. Phase space cuts used for the theoretical predictions in our study.

	$\sigma_{\gamma+Q}^{pp}$ [pb]	$\sigma_{\gamma+Q}^{PbPb}$ [nb]	$N_{\gamma+Q}^{PbPb}$
$\gamma + c$ (noEL)	112.5	4820	2410
$\gamma + c$ ($\omega_c = 50 \text{ GeV}$)	98	4200	2100
$\gamma + c$ ($\omega_c = 100 \text{ GeV}$)	83	3556	1778
$\gamma + b$ (noEL)	15.5	664	332
$\gamma + b$ ($\omega_c = 50 \text{ GeV}$)	14.7	630	315
$\gamma + b$ ($\omega_c = 100 \text{ GeV}$)	14.4	617	308

Table 3. Total integrated cross section and number of events per year for $\gamma + Q$ production in Pb–Pb collisions at the LHC.

3.2 Total cross sections and event rates

In this section we compute the NLO cross sections for $p+p \rightarrow \gamma+c+X$ and $p+p \rightarrow \gamma+b+X$ taking into account the cuts on the phase space listed in Table 2. The corresponding cross sections for Pb–Pb collisions are obtained by scaling the ones for p–p collisions with A^2 where $A = 207$ is the atomic number of lead. In Table 3, we present results for the cross section in vacuum and for two media with parameters $R = 10^5$, $\omega_c = 50 \text{ GeV}$ and $R = 10^5$, $\omega_c = 100 \text{ GeV}$, respectively. The expected number of events per year are given in the third column assuming a yearly luminosity of $\mathcal{L}_{PbPb}^{\text{year}} = 0.5 \text{ nb}^{-1}$ for Pb–Pb collisions at the LHC [43]. As can be seen, the event numbers are sufficiently large to measure the cross section for both, $\gamma + c$ and $\gamma + b$ production where the $\gamma + b$ cross section is roughly a factor of 7 smaller. The smaller cross sections in medium are due to the fact that fewer events pass the cut $p_{TQ} > p_{T,Q}^{min}$ when energy loss is present. With sufficiently large statistics, it could also be interesting to analyze the cross section as a function of $p_{T,Q}^{min}$. The $\gamma + c$ cross section clearly depends on ω_c . The suppression factor of the total cross section is given by $R_{AA} = 0.87$ ($R_{AA} = 0.74$) for $\omega_c = 50 \text{ GeV}$ ($\omega_c = 100 \text{ GeV}$). Conversely, the dependence of the $\gamma + b$ cross section on ω_c is much more modest with $R_{AA} = 0.95$ ($R_{AA} = 0.93$) for $\omega_c = 50 \text{ GeV}$ ($\omega_c = 100 \text{ GeV}$). It is noteworthy that the suppression effect could be further enhanced by optimizing the values for the cuts on $p_{T\gamma}$ and p_{TQ} . In particular, the quenching could be enhanced (without reducing the cross section too much) by imposing an upper integration bound $p_{T\gamma} < p_{T,\gamma}^{max} \lesssim 50 \text{ GeV}$ as can be inferred from Fig. 1(a).

The numbers in Table 3 can be used to obtain rough estimates of cross sections and event rates when other phase space cuts are employed or detection efficiencies for the photon and the heavy quark are taken into account: (i) Assuming an approximately flat rapidity dependence, the cross section will roughly scale with the size of the rapidity bins of the photon and the heavy quark jet. We checked that using $|y_\gamma| < 2$ and $|y_Q| < 2$ leads

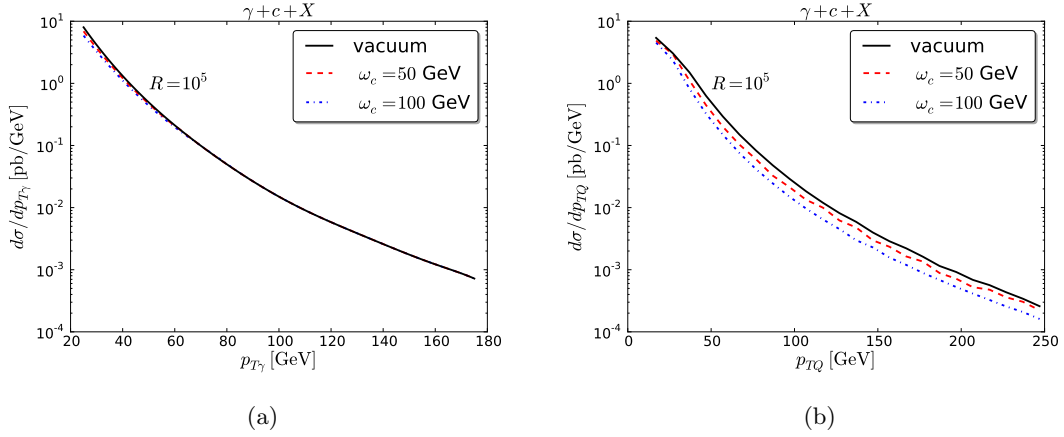


Figure 1. Next-to-leading order differential cross section a) $d\sigma/dp_{T\gamma}$ as a function of $p_{T\gamma}$ and b) $d\sigma/dp_{TQ}$ as a function of p_{TQ} in pb/GeV. Shown are results for the vacuum (black solid lines) and for different media with $R = 10^5$ and $\omega_c = 50$ (red dashed lines) and 100 GeV (blue dash-dotted lines).

to a cross section roughly 60 times larger than the one quoted in Table 3; (ii) Assuming a power-law behavior for the $p_{T\gamma}$ and p_{TQ} dependence (see Sec. 3.3.2) the cross sections will depend strongly on the values of $p_{T,\gamma}^{min}$ and $p_{T,Q}^{min}$. Results for $p_{T,\gamma}^{min}$ and $p_{T,Q}^{min}$ different from the ones in Table 2 can be estimated by multiplying the cross sections/event numbers with a factor $(12 \text{ GeV}/p_{T,Q}^{min})^n \times (20 \text{ GeV}/p_{T,\gamma}^{min})^n$ with $n \simeq 4$.

While a more precise estimate of the expected event numbers clearly depends on the details of the experimental acceptances and efficiencies our results indicate that the number of $\gamma + c$ events produced in a year of Pb–Pb collisions at the LHC will be substantial and that also a measurement of the $\gamma + b$ cross section will be feasible before the projected upgrade of the luminosity during the second long shutdown of the LHC where an instantaneous luminosity $\mathcal{L}_{\text{PbPb}}^{\text{inst}} = 6 \times 10^{27} \text{ cm}^{-2} \text{ s}^{-1}$ is expected [44] corresponding to a yearly ($t = 10^6 \text{ s}$) luminosity of $\mathcal{L}_{\text{PbPb}}^{\text{year}} = 6 \text{ nb}^{-1}$.

3.3 Single-inclusive transverse momentum spectra

3.3.1 Differential cross sections

Before turning to the nuclear production ratios, we first present the predictions for the single p_T spectra in p–p and Pb–Pb collisions. In Fig. 1 the NLO differential cross sections $d\sigma/dp_{T\gamma}$ (left) and $d\sigma/dp_{TQ}$ (right) for $\gamma + c$ production are shown for the vacuum and for different media ($\omega_c = 50$ and 100 GeV, with $R = 10^5$). As discussed in Sec. 2, in our framework the photon is not affected by the medium. However, as can be seen in Fig. 1(a), at small $p_{T\gamma}$, the $p_{T\gamma}$ spectrum in medium is reduced below the vacuum spectrum. The reason is that fewer events pass the cut on the heavy quark jet transverse momentum ($p_{TQ} > 12 \text{ GeV}$), if heavy quark energy loss is present. This is a physical effect which scales with the heavy quark energy loss at small $p_{T\gamma}$: at $\omega_c = 50 \text{ GeV}$ ($\omega_c = 100 \text{ GeV}$) we

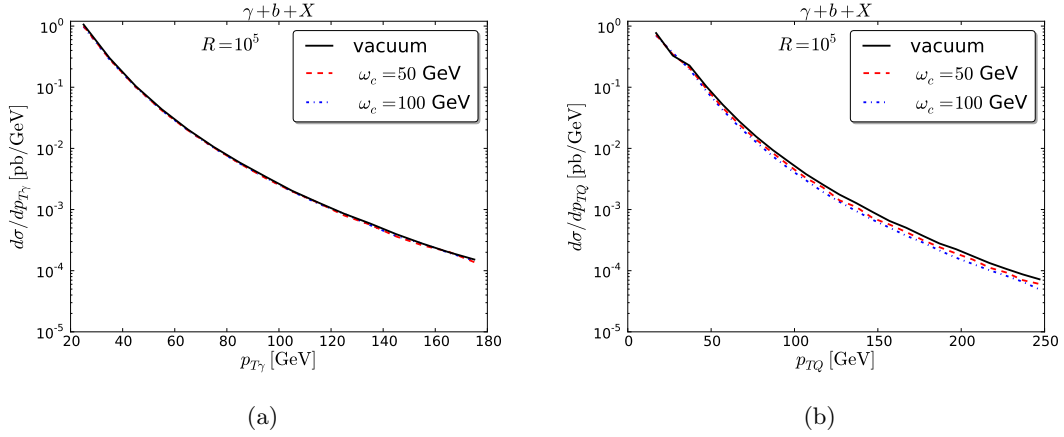


Figure 2. Same as in Fig. 1 for the $\gamma + b$ case.

observe a 15% (30%) reduction. Conversely $R_{AA}^{p_{T\gamma}}$ is unity at values away from the cut, say for $p_{T\gamma} \gtrsim 70$ GeV, since for these momenta most of the heavy quark jets pass the cuts as $p_{TQ} \gg p_{TQ}^{\text{cut}}$.

The p_{TQ} spectra are much more affected by the medium over the entire p_T range, as is clearly visible in Fig. 1(b). In this case, the quenching is not related to the presence of the heavy quark threshold required in the calculation but rather due to the shift of the jet momentum, see Eq. (2.4), in heavy-ion collisions. At $p_{TQ} \lesssim 50$ GeV the heavy quark mass mildens the energy loss effects, leading to a small difference between the vacuum cross section (black solid line) and the in medium cross sections (red dashed line, blue dash-dotted line). This will be further discussed in the next section where quenching factors are presented.

In Fig. 2 we present the same observables, but for $\gamma + b$ production. As is visible the same trends are present as in Fig. 1, which are however clearly reduced in size compared to the $\gamma + c$ case.

3.3.2 Quenching factors R_{AA}

We consider here the quenching factor $R_{AA}^Q(p_{TQ})$ of the heavy-quark jet. The goal is twofold. Firstly, as mentioned in Section 2.3, the aim is to show the sensitivity of the observables involving a photon and heavy quark jet in the final state on parton energy losses entering via different (massless and massive) quenching weights. Secondly, we want to explore the effects of the NLO QCD corrections on the quenching factor $R_{AA}^Q(p_{TQ})$.

As an illustration of the first point, the quenching of the charm jet p_T spectrum in $\gamma + c$ production has been computed as a function of p_{Tc} in Fig. 3(a) under various hypothesis regarding the energy loss of charm quarks, i.e. assuming that the charm quark suffers the same energy loss as that of a light quark (blue dash-dotted line) or that of a heavy quark assuming $m_Q = m_c$ (red dashed line) and $m_Q = m_b$ (black solid line) in the quenching weights (for completeness the calculation has also been carried out using the quenching

weight of a propagating gluon, brown dotted line). The calculation is performed at leading order direct, i.e. according to the Compton subprocess only. The quenching factors computed using these various prescriptions follow closely the hierarchy of parton energy loss in the BDMPS-Z quenching weights used for each flavor in the calculation, which are shown in Fig. 3(b). In particular, a much stronger (respectively, weaker) charm jet quenching would be expected should the charm quark lose energy like a gluon (respectively, bottom quark). Interesting also is the comparison between the predictions assuming light quark and charm quark energy loss. At low transverse momenta, the charm quark energy loss predicts less suppression as compared to the light quark energy loss, which is comparable in size to the suppression of inclusive D meson production as recently measured for example in [45]. At large momenta on the other hand, $p_{Tc} \gg m_c$, the induced energy loss of a charm and a light quark become identical, as can be seen in Fig. 3(a) (by comparing the dashed and dash-dotted lines).¹⁰

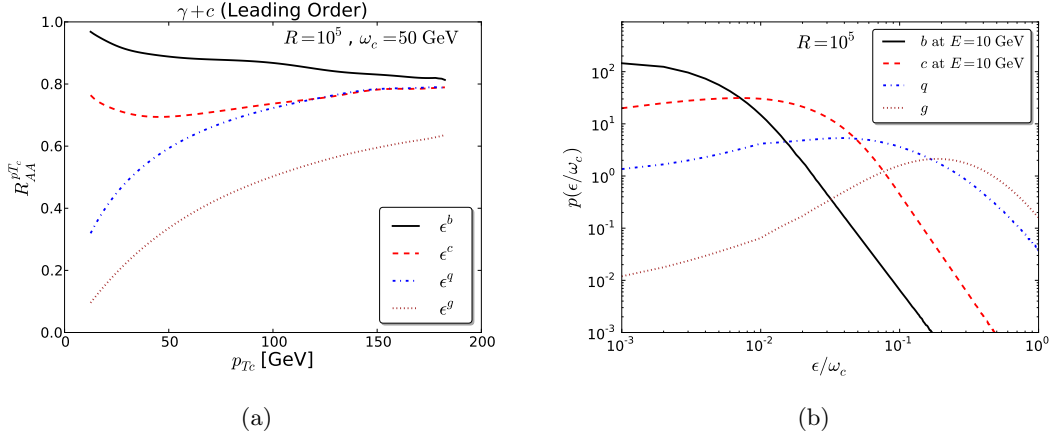


Figure 3. a) Suppression factors R_{AA} in leading order versus transverse charm momentum, p_{Tc} , applying energy loss according to the quenching weights shown in the right figure; b) Quenching weights for energy loss corresponding to gluons (dotted, brown line), light quarks (dash-dotted, blue line), charm quarks (dashed, red line), and bottom quarks (solid, black line) in dependence of the energy loss ϵ scaled to ω_c .

It is possible to extract information on the parton energy loss from the suppression factors R_{AA} in Fig. 3(a), by assuming a power law dependence of the differential cross section $d\sigma/dp_{TQ}$ vs. p_{TQ} :

$$\frac{d\sigma^{\text{vac}}}{dp_{TQ}} \propto p_{TQ}^{-n} \quad (3.1)$$

where the index n increases smoothly from $n \simeq 4$ to $n \simeq 5.5$ from low to high transverse momenta. The medium cross section is obtained by shifting the transverse momentum by

¹⁰Similarly, the solid black line merges with the quenching factor for light quarks at even larger p_{Tc} .

	p_{TQ}	R_{AA}	n	$\tilde{\epsilon}$ (GeV)	$\tilde{\epsilon}/\omega_c$	$\epsilon^{\text{peak}}/\omega_c$	$\langle\epsilon^{\text{qw}}\rangle/\omega_c$
b	30	0.90	4.0	0.8	0.016	0.008	0.022
c	30	0.69	4.0	2.9	0.058	0.025	0.08
q	30	0.49	4.0	6.0	0.12	0.04	0.18
g	30	0.23	4.0	13.5	0.27	0.19	0.4
b	90	0.87	5.5	2.3	0.046	0.026	0.069
c	90	0.72	5.5	5.6	0.11	0.036	0.18
q	90	0.70	5.5	6.0	0.12	0.04	0.18
g	90	0.48	5.5	13.0	0.26	0.19	0.4

Table 4. Extracted energy loss (column 4) from the nuclear suppression factor R_{AA} (column 2) in Fig. 3(a) using Eq. (3.4) for bottom, charm, light quark, and gluon energy loss, at two different p_{TQ} values (column 1). For comparison the peak energy loss (column 6) and the mean energy loss (column 7) scaled to $\omega_c = 50$ GeV are shown as well, see text for details.

a *typical* transverse energy loss $\tilde{\epsilon}_T$ (which could have a p_{TQ} dependence):

$$\frac{d\sigma^{\text{med}}}{dp_{TQ}^{\text{med}}}(p_{TQ}^{\text{med}}) \simeq \frac{d\sigma^{\text{vac}}}{dp_{TQ}}(p_{TQ} = p_{TQ}^{\text{med}} + \tilde{\epsilon}_T). \quad (3.2)$$

As a consequence the suppression factor is approximately given by

$$R_{AA}^Q(p_{TQ}) = \left(\frac{p_{TQ}}{p_{TQ} + \tilde{\epsilon}_T} \right)^n, \quad (3.3)$$

leading to

$$\tilde{\epsilon}_T = p_{TQ} \left((R_{AA}^Q)^{-1/n} - 1 \right), \quad \tilde{\epsilon} = \tilde{\epsilon}_T \cosh y_Q. \quad (3.4)$$

Using Eq. (3.4) and the values for R_{AA} in Fig. 3(a) at $p_{TQ} = 30$ GeV (taking $n = 4$) and $p_{TQ} = 90$ GeV ($n = 5.5$) we obtain the energy loss values $\tilde{\epsilon}$ presented in column four¹¹ of Table 4 (in the fifth column the value is scaled by $\omega_c = 50$ GeV). We compare this to the energy loss corresponding to the peak of the quenching weights for bottom, charm, light quark and gluons in column 6. Finally in the seventh column we show the energy loss corresponding to the mean of these quenching weights.

It is interesting to note that the ratio of the energy loss for gluon and light quarks (13.5/6.0 or 13.0/6.0) is very close to the ratio of the color factors $C_A/C_F = 9/4$. As can be seen the energy loss for light quarks and gluons is independent of the chosen p_{TQ} value, whereas the heavy quarks lose less energy at small p_{TQ} due to the mass effects. Furthermore at $p_{TQ} = 90$ GeV the charm quark energy loss is already almost identical to the light quark one. As can be seen the extracted values for the energy loss (in column five) are systematically larger (by a factor varying between 1.4 and 3.0) than the most likely (“peak”) energy loss according to the quenching weights (in column 6) and systematically smaller (by a factor varying between 1.2 and 1.6) than the average energy loss.

¹¹Note that $\tilde{\epsilon} \simeq \tilde{\epsilon}_T$ for central rapidities $|y| < 0.2$.

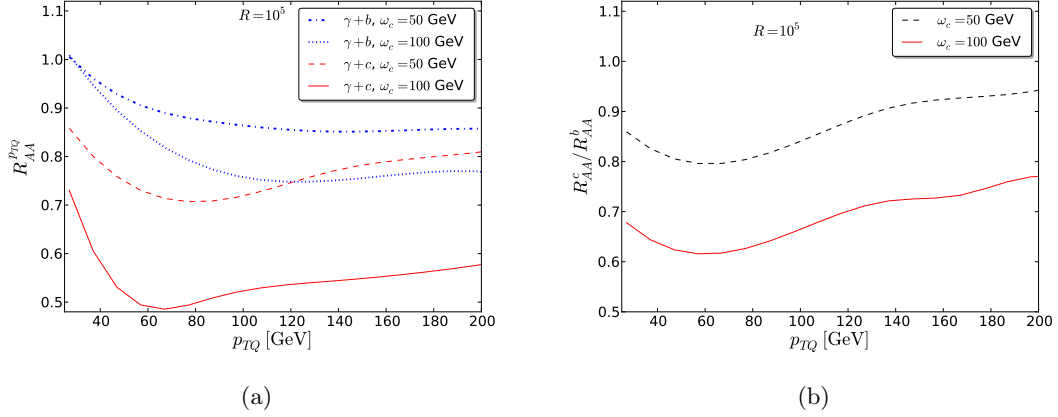


Figure 4. a) R_{AA}^{pTQ} for $\gamma + c$ and $\gamma + b$ production at NLO QCD. b) Double ratio R_{AA}^c/R_{AA}^b for $\omega_c = 50$ (dashed line) and 100 GeV (solid line).

Now turning to the NLO results, we present predictions for the quenching factors R_{AA} for both, $\gamma + c$ (red dashed and solid lines) and $\gamma + b$ (blue dotted and dash-dotted lines) production, in Fig. 4(a). It is reassuring to see that the quenching factors at NLO are not very different from the ones obtained at LO (compare, for example, the red dashed lines in Figs. 4(a) and 3(a)). The corresponding double ratios R_{AA}^c/R_{AA}^b for $\omega_c = 50$ (dashed line) and 100 GeV (solid line) are shown in Fig. 4(b). Clearly, the double ratio for $\omega_c = 100$ GeV is much smaller than the one for $\omega_c = 50$ GeV implying a strong sensitivity to the energy loss of the charm and bottom quark jets in the medium. Interestingly, the two double ratios have a very similar shape for both values of ω_c .

3.4 Two-particle observables

We now turn to a discussion of the two-particle observables introduced in Sec. 2.4. We begin with the q_T distribution defined in Eq. (2.8) for $\gamma + c$ production which is shown in Fig. 5(a) for negative and in Fig. 5(b) for positive values of q_T . We have spared the region $-20 \text{ GeV} \leq q_T \leq 20 \text{ GeV}$ where $p_{T\gamma} \simeq p_{TQ}$ to avoid problems with IR-safety¹² as discussed in Sec. 3.1. In addition to the vacuum cross section (black solid line) results are shown for a medium with $\omega_c = 50$ GeV (red dashed line) respectively $\omega_c = 100$ GeV (blue dash-dotted line). As can be seen the medium spectra are right-shifted with respect to the vacuum one for both, negative and positive values of q_T (see the discussion in Sec. 2.4). Clearly, the shift increases with increasing ω_c and is smaller for positive q_T where it is about 2 GeV for $\omega_c = 50$ GeV and varying between 3.5 and 5 GeV for $\omega_c = 100$ GeV. For negative q_T the shift is roughly 5 GeV (11–15 GeV) for $\omega_c = 50$ GeV ($\omega_c = 100$ GeV). The overall differences in shape and size of the curves in Figs. 5(a) and 5(b) can be understood as a consequence of

¹²Note that meaningful results can still be obtained when integrating/binning over a sufficiently large region around $q_T = 0$ as has been done in Fig. 9 for the observables A_J (binning around $A_J = 0$) and z (binning around $z = 1$).

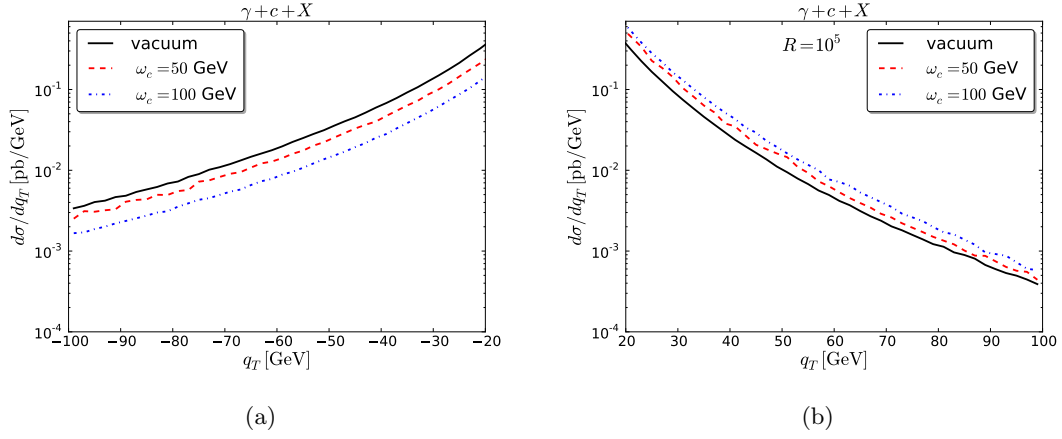


Figure 5. Next-to-leading order differential cross section $d\sigma/dq_T$ for the production of $\gamma + c$ for a) negative and b) positive values of q_T . Shown are results for the vacuum (black solid lines) and for different media with $R = 10^5$ and $\omega_c = 50$ (red dashed lines) and 100 GeV (blue dash-dotted lines).

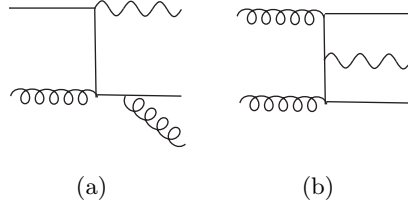


Figure 6. Feynman diagrams for the subprocesses a) $gQ \rightarrow gQ\gamma$ and b) $gg \rightarrow Q\bar{Q}\gamma$ giving the main contribution to the q_T distributions in Figs. 5 and 8 at *positive* values of q_T .

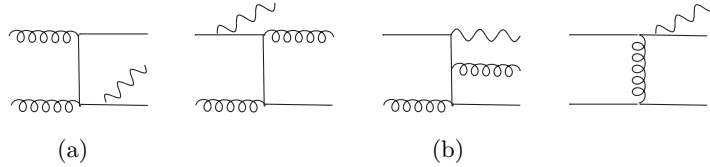


Figure 7. Feynman diagrams for the subprocesses a) $gg \rightarrow Q\bar{Q}\gamma$ and b) $gQ \rightarrow gQ\gamma$ and $qQ \rightarrow qQ\gamma$ giving the main contribution to the q_T distributions in Figs. 5 and 8 at *negative* values of q_T .

the different subprocesses which contribute (dominantly) to the cross section for positive and negative q_T . For positive q_T , the dominant contribution comes from the subprocess $gQ \rightarrow gQ\gamma$ followed by $gg \rightarrow Q\bar{Q}\gamma$ where appropriate Feynman diagrams are shown in Figs. 6(a) and 6(b), respectively, where the leading photon is balanced by the Qg pair in Fig. 6(a) and by the $Q\bar{Q}$ pair in Fig. 6(b). For negative q_T , the dominant contribution comes from the subprocess $gg \rightarrow Q\bar{Q}\gamma$ where in this case the relevant Feynman diagram is

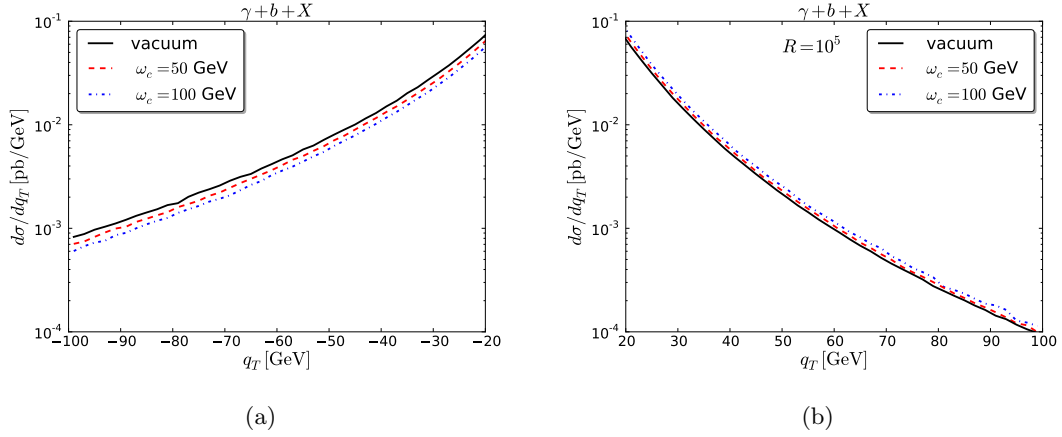


Figure 8. Same as in Fig. 5 for $\gamma + b$ production.

shown in Fig. 7(a) for a leading heavy quark jet.¹³ Other non-negligible subprocesses (for $q_T < 0$) are $gQ \rightarrow gQ\gamma$ and $qQ \rightarrow qQ\gamma$ (see Fig. 7(b) for sample diagrams).

The larger shift in energy for negative q_T (compared to the positive q_T case) can be understood in the following way: the photon momentum $p_{T\gamma}$ remains fixed close to its minimal value $p_{T\gamma}^{\min} = 20$ GeV whereas p_{TQ} varies (i.e. is larger) in order to satisfy $q_T \simeq p_{T\gamma}^{\min} - p_{TQ}$. Hence the heavy quark energy loss is less pronounced since mass effects are less important at larger p_{TQ} values. Conversely, for $q_T > 0$, the situation is inverted where now p_{TQ} remains fixed close to its minimal value $p_{TQ}^{\min} = 12$ GeV whereas $p_{T\gamma}$ varies (i.e. is larger) in order to satisfy $q_T \simeq p_{T\gamma} - p_{TQ}^{\min}$. In this case, the heavy quark energy loss will be smaller because the heavy quark mass effects are still relevant. In Fig. 8 we present the corresponding results for $\gamma + b$ production. Again, the same trends can be observed which are, however, reduced in size.

Finally, in Fig. 9 we show results for the jet asymmetry A_J (left) and the momentum imbalance z (right). The variable A_J defined in Eq. (2.9) is very similar to q_T and the A_J spectrum shows indeed very similar features as the q_T distribution, in particular the in-medium curves are shifted to the right, the shift is larger for negative A_J , and the distribution is slightly asymmetric around $A_J = 0$. The z -distribution peaks at $z = 1$ which corresponds to a configuration where the heavy quark and the photon are back-to-back (as in LO). With our cut on the angle between the heavy quark jet and the photon momentum ($\theta > 3\pi/4$) we find $0.7 \times \frac{p_{TQ}}{p_{T\gamma}} \leq z = -\frac{p_{TQ}}{p_{T\gamma}} \cos \theta \leq \frac{p_{TQ}}{p_{T\gamma}}$. Therefore, roughly, the region $z < 1$ ($z > 1$) corresponds to $p_{TQ} < p_{T\gamma}$ ($p_{TQ} > p_{T\gamma}$). In this case, the in-medium spectra are left-shifted and the bigger shifts are visible in the region $z > 1$ which corresponds, as in the previous figures, to the kinematic configuration $p_{TQ} > p_{T\gamma}$.

¹³Note that this amplitude is suppressed in the case of positive q_T because we require that the tagged heavy quark be the one with the largest p_T .

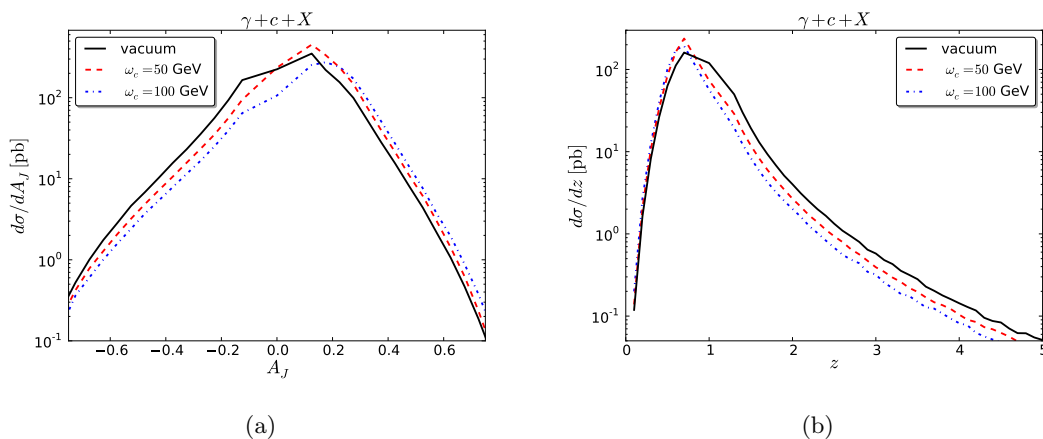


Figure 9. Differential cross section with respect to a) the jet asymmetry A_J and b) the momentum imbalance z into the $\gamma + c$ production channel.

4 Conclusions

An important aspect of jet quenching phenomenology is to understand the mass dependence of parton energy loss. While the quenching of single inclusive hadron production might give a clue on this topic, the possibilities offered by the LHC experiments allow for investigating more exclusive processes which have the advantage that a range of interesting observables can be constructed from the momenta of the final state particles.

In this paper, we performed an exploratory study of the associated production of a photon and a heavy quark jet in heavy-ion collisions, at NLO accuracy. On general grounds this is a very promising process in which the energy loss of the heavy quark jet can be calibrated using the prompt photon momentum since the latter is assumed to be unaffected by the hot and dense QCD medium. Despite the smaller cross sections as compared to the single inclusive heavy-quark jet production, the expected rate at the LHC is sufficiently large to ensure reasonable statistical uncertainties for both $\gamma + c$ and $\gamma + b$ production. In addition to the inclusive p_T spectra of the photon and the heavy quark jet, we have performed NLO calculations for a range of observables (q_T , A_J , z) in order to identify which of these distributions provide useful information on the amount of energy loss experienced by the propagating heavy quark.

The inclusive p_{TQ} and $p_{T\gamma}$ distributions are very promising observables. Numerical results for $d\sigma/dp_{T\gamma}$ and $d\sigma/dp_{TQ}$ calculated at NLO QCD were presented. We find that the p_{TQ} spectra are affected by the medium over the entire p_T range, whereas the $p_{T\gamma}$ distribution only gets quenched at small $p_{T\gamma}$ due to the cut on the jet transverse momentum. Comparing these two spectra should thus be particularly instructive in order to disentangle the effects due to the heavy-quark energy loss from the ones due to the nuclear modification of the parton distribution functions and other cold nuclear matter effects. Information on the parton energy loss could be obtained either by studying the total cross section as a function of the cut on the jet transverse momentum or by analyzing the p_{TQ} distribution.

For the latter we have presented in Fig. 4(a) the quenching factors R_{AA} for both, $\gamma + c$ and $\gamma + b$ production at NLO QCD. Very interesting is also the double ratio R_{AA}^c/R_{AA}^b shown in Fig. 4(b) of which the *shape* (not the normalization) as function of $p_{TQ} = p_{Tc} = p_{Tb}$ turns out to be almost independent of the choice of the parameter ω_c .

The distributions in the two-particle kinematic variables have also been investigated in detail, paying attention in particular to the photon-jet pair momentum q_T . As expected, these distributions are shifted towards larger values in heavy-ion collisions. The comparison of q_T spectra in p-p and Pb-Pb collisions for $\gamma + c$ and $\gamma + b$ production should thus allow for a “direct” access to the amount of energy lost by charm and bottom quarks, respectively. Note that such distributions are singular at leading order accuracy and therefore NLO predictions prove mandatory in order to compute such spectra at large (positive and negative) q_T values.

For completeness the distributions in the photon-jet asymmetry, A_J , and momentum imbalance, z , have also been determined in the $\gamma + c$ channel in p-p and Pb-Pb collisions. Similar patterns to the ones observed in the q_T distributions are reported. The comparison between the distributions in various kinematic variables should thus help to determine at a quantitative level the amount of heavy-quark energy loss from the future high-precision measurements through detailed phenomenological studies.

Let us mention some future improvements to be carried out beyond the present study. The systematic comparison of $\gamma + c/b$ jet production with $\gamma +$ *inclusive* jet production (for which first measurements have been reported recently [8]) should be particularly interesting and useful. In addition, as soon as the nuclear gluon parton distribution is better constrained from data of the forthcoming p-A run at the LHC, the predictions should be updated using *nuclear* PDFs including systematic studies of the nPDF and scale uncertainties. Finally, it would also be important to compare the present calculations with calculations based on other energy loss frameworks and different assumptions regarding the modeling of the heavy-quark energy loss in the medium.

Acknowledgment

We are grateful to thank S. Peigné for useful discussions on parton energy loss. This work was supported by the CNRS through a PICS research grant and the Théorie-LHC-France initiative. This work is funded by “Agence Nationale de la Recherche” under grant ANR-PARTONPROP.

References

- [1] **ALICE** Collaboration, K. Aamodt *et. al.*, *Suppression of Charged Particle Production at Large Transverse Momentum in Central Pb–Pb Collisions at $\sqrt{s_{NN}} = 2.76$ TeV*, *Phys. Lett. B* **696** (2011) 30, [[1012.1004](#)].
- [2] **ATLAS** Collaboration, *Measurement of the centrality dependence of charged particle spectra and rcp in lead-lead collisions at $s_{nn} = 2.76$ tev with the atlas detector at the lhc*, Tech. Rep. ATLAS-CONF-2011-079, CERN, Geneva, Jun, 2011.
- [3] **CMS** Collaboration, S. Chatrchyan *et. al.*, *Study of high- p_T charged particle suppression in Pb–Pb compared to p – p collisions at $\sqrt{s_{NN}} = 2.76$ TeV*, *Eur. Phys. J.* **C72** (2012) 1945, [[1202.2554](#)].
- [4] **ALICE Collaboration** Collaboration, Z. Conesa del Valle, *D mesons suppression in PbPb collisions at $\sqrt{s_{NN}} = 2.76$ TeV measured by ALICE*, [1210.2163](#).
- [5] **ATLAS** Collaboration, *Measurement of the centrality dependence of open heavy flavour production in lead-lead collisions at $\sqrt{s} = 2.76$ tev with the atlas detector*, Tech. Rep. ATLAS-CONF-2012-050, CERN, Geneva, May, 2012.
- [6] **ATLAS** Collaboration, G. Aad, *Observation of a Centrality-Dependent Dijet Asymmetry in Lead-Lead Collisions at $\sqrt{s_{NN}} = 2.76$ TeV with the ATLAS Detector at the LHC*, *Phys. Rev. Lett.* **105** (2010) 252303, [[1011.6182](#)].
- [7] **CMS** Collaboration, S. Chatrchyan *et. al.*, *Observation and studies of jet quenching in PbPb collisions at nucleon-nucleon center-of-mass energy = 2.76 TeV*, *Phys.Rev.* **C84** (2011) 024906, [[1102.1957](#)].
- [8] **CMS** Collaboration, S. Chatrchyan *et. al.*, *Studies of jet quenching using isolated-photon+jet correlations in PbPb and pp collisions at $\sqrt{s_{NN}} = 2.76$ TeV*, [1205.0206](#).
- [9] **ATLAS** Collaboration, *Measurement of momentum imbalance in $z \rightarrow \ell\ell + \text{jet}$ events in lead-lead collisions at $\sqrt{s_{NN}} = 2.76$ tev with the atlas detector*, Tech. Rep. ATLAS-CONF-2012-119, CERN, Geneva, Aug, 2012.
- [10] **CMS Collaboration** Collaboration, S. Chatrchyan *et. al.*, *Measurement of jet fragmentation into charged particles in pp and PbPb collisions at $\sqrt{s(s[NN])} = 2.76$ TeV*, *JHEP* **1210** (2012) 087, [[1205.5872](#)].
- [11] **ATLAS** Collaboration, *Measurement of inclusive jet charged particle fragmentation functions in pb+pb collisions at $\sqrt{s(s[nn])} = 2.76$ tev with the atlas detector*, Tech. Rep. ATLAS-CONF-2012-115, CERN, Geneva, Aug, 2012.
- [12] Y. L. Dokshitzer and D. Kharzeev, *Heavy quark colorimetry of QCD matter*, *Phys.Lett. B* **519** (2001) 199–206, [[hep-ph/0106202](#)].
- [13] N. Armesto, C. A. Salgado, and U. A. Wiedemann, *Medium-induced gluon radiation off massive quarks fills the dead cone*, *Phys. Rev. D* **69** (2004) 114003.
- [14] P. Aurenche and B. Zakharov, *Anomalous mass dependence of radiative quark energy loss in a finite-size quark-gluon plasma*, *JETP Lett.* **90** (2009) 237–243, [[0907.1918](#)].
- [15] **D0** Collaboration, V. M. Abazov *et. al.*, *Measurement of $\gamma + b + X$ and $\gamma + c + X$ production cross sections in $p\bar{p}$ collisions at $\sqrt{s} = 1.96$ TeV*, *Phys. Rev. Lett.* **102** (2009) 192002, [[0901.0739](#)].

- [16] **CDF** Collaboration, T. Aaltonen *et. al.*, *A Study of the associated production of photons and b-quark jets in $p\bar{p}$ collisions at $\sqrt{s} = 1.96$ TeV*, *Phys.Rev.* **D81** (2010) 052006, [[0912.3453](#)].
- [17] **D0** Collaboration, V. M. Abazov *et. al.*, *Measurement of the photon+b-jet production differential cross section in $p\bar{p}$ collisions at $\sqrt{s} = 1.96$ TeV*, *Phys.Lett.* **B714** (2012) 32–39, [[1203.5865](#)].
- [18] **D0** Collaboration, V. M. Abazov *et. al.*, *Measurement of differential photon+ c-jet cross sections and the ratio of photon+ c and photon+ b cross sections in proton-antiproton collisions at $\sqrt{s} = 1.96$ TeV*, [1210.5033](#).
- [19] T. Stavreva and J. Owens, *Direct Photon Production in Association With A Heavy Quark At Hadron Colliders*, *Phys.Rev.* **D79** (2009) 054017, [[0901.3791](#)].
- [20] T. Stavreva, I. Schienbein, F. Arleo, K. Kovarik, F. Olness, *et. al.*, *Probing gluon and heavy-quark nuclear PDFs with $\gamma + Q$ production in pA collisions*, *JHEP* **1101** (2011) 152, [[1012.1178](#)].
- [21] Z.-B. Kang and I. Vitev, *Photon-tagged heavy meson production in high energy nuclear collisions*, *Phys.Rev.* **D84** (2011) 014034, [[1106.1493](#)].
- [22] F. Arleo, P. Aurenche, Z. Belghobsi, and J.-P. Guillet, *Photon tagged correlations in heavy ion collisions*, *JHEP* **11** (2004) 009, [[hep-ph/0410088](#)].
- [23] H. Zhang, J. F. Owens, E. Wang, and X.-N. Wang, *Tomography of high-energy nuclear collisions with photon- hadron correlations*, *Phys. Rev. Lett.* **103** (2009) 032302, [[0902.4000](#)].
- [24] W. Dai, I. Vitev, and B.-W. Zhang, *Momentum imbalance of isolated photon-tagged jet production at RHIC and LHC*, [1207.5177](#).
- [25] T. Stavreva, *Direct photon production in association with a heavy quark*. PhD thesis, Florida State University, 2009. URN: etd-04102009-155714.
- [26] Y. Mehtar-Tani, C. A. Salgado, and K. Tywoniuk, *Anti-angular ordering of gluon radiation in QCD media*, *Phys.Rev.Lett.* **106** (2011) 122002, [[1009.2965](#)].
- [27] N. Armesto, H. Ma, Y. Mehtar-Tani, C. A. Salgado, and K. Tywoniuk, *Coherence effects and broadening in medium-induced QCD radiation off a massive $q\bar{q}$ antenna*, *JHEP* **1201** (2012) 109, [[1110.4343](#)].
- [28] J. Casalderrey-Solana, J. G. Milhano, and P. Q. Arias, *Out of Medium Fragmentation from Long-Lived Jet Showers*, *Phys.Lett.* **B710** (2012) 175–181, [[1111.0310](#)].
- [29] J. Casalderrey-Solana, Y. Mehtar-Tani, C. A. Salgado, and K. Tywoniuk, *New picture of jet quenching dictated by color coherence*, [1210.7765](#).
- [30] R. Baier, Y. L. Dokshitzer, A. H. Mueller, and D. Schiff, *Quenching of hadron spectra in media*, *JHEP* **0109** (2001) 033, [[hep-ph/0106347](#)].
- [31] U. A. Wiedemann, *Gluon radiation off hard quarks in a nuclear environment: Opacity expansion*, *Nucl.Phys.* **B588** (2000) 303–344, [[hep-ph/0005129](#)].
- [32] R. Baier, Y. L. Dokshitzer, A. H. Mueller, S. Peigne, and D. Schiff, *Radiative energy loss of high-energy quarks and gluons in a finite volume quark - gluon plasma*, *Nucl.Phys.* **B483** (1997) 291–320, [[hep-ph/9607355](#)].
- [33] C. A. Salgado and U. A. Wiedemann, *Calculating quenching weights*, *Phys.Rev.* **D68** (2003) 014008, [[hep-ph/0302184](#)].

- [34] N. Armesto, A. Dainese, C. A. Salgado, and U. A. Wiedemann, *Testing the color charge and mass dependence of parton energy loss with heavy-to-light ratios at RHIC and CERN LHC*, *Phys.Rev.* **D71** (2005) 054027, [[hep-ph/0501225](#)].
- [35] **CMS Collaboration**, S. Chatrchyan *et. al.*, *Jet momentum dependence of jet quenching in PbPb collisions at $\sqrt{s_{NN}} = 2.76$ TeV*, *Phys.Lett.* **B712** (2012) 176–197, [[1202.5022](#)].
- [36] F. Arleo, *Hard pion and prompt photon at RHIC, from single to double inclusive production*, *JHEP* **09** (2006) 015, [[hep-ph/0601075](#)].
- [37] K. J. Eskola, H. Paukkunen, and C. A. Salgado, *EPS09 - A New Generation of NLO and LO Nuclear Parton Distribution Functions*, *JHEP* **04** (2009) 065, [[0902.4154](#)].
- [38] M. Hirai, S. Kumano, and T. H. Nagai, *Determination of nuclear parton distribution functions and their uncertainties at next-to-leading order*, *Phys. Rev.* **C76** (2007) 065207, [[0709.3038](#)].
- [39] I. Schienbein, J. Yu, K. Kovarik, C. Keppel, J. Morfin, *et. al.*, *PDF Nuclear Corrections for Charged and Neutral Current Processes*, *Phys.Rev.* **D80** (2009) 094004, [[0907.2357](#)].
- [40] D. de Florian, R. Sassot, P. Zurita, and M. Stratmann, *Global Analysis of Nuclear Parton Distributions*, *Phys.Rev.* **D85** (2012) 074028, [[1112.6324](#)].
- [41] P. M. Nadolsky, H.-L. Lai, Q.-H. Cao, J. Huston, J. Pumplin, *et. al.*, *Implications of CTEQ global analysis for collider observables*, *Phys.Rev.* **D78** (2008) 013004, [[0802.0007](#)].
- [42] L. Bourhis, M. Fontannaz, and J. Guillet, *Quarks and gluon fragmentation functions into photons*, *Eur.Phys.J.* **C2** (1998) 529–537, [[hep-ph/9704447](#)].
- [43] F. Arleo *et. al.*, *Photon physics in heavy ion collisions at the LHC*, [hep-ph/0311131](#).
- [44] **ALICE Collaboration**, B. Abelev *et al.*, “Upgrade of the ALICE Experiment. Letter Of Intent.” <http://cdsweb.cern.ch/record/1475243/files/LHCC-I-022.pdf>, 2012.
- [45] **ALICE Collaboration**, B. Abelev *et. al.*, *Suppression of high transverse momentum D mesons in central Pb-Pb collisions at $\sqrt{s_{NN}} = 2.76$ TeV*, *JHEP* **1209** (2012) 112, [[1203.2160](#)].